



Stem and root assessment in mangrove forests using a low-cost, rapid-scan terrestrial laser scanner

Ali Rouzbeh Kargar · Richard A. MacKenzie · Maybeleen Apwong · Ethan Hughes · Jan van Aardt

Received: 26 November 2019 / Accepted: 21 September 2020 / Published online: 3 November 2020
© Springer Nature B.V. 2020

Abstract Accurate assessment of forest structure and biomass is hampered by extensive field measurements that are time-consuming, costly, and inefficient. This is especially true in mangrove forests that have developed complex above-ground root structures for stability and survival in the harsh, anaerobic, and reducing conditions of water-logged sediments. These diverse structures can differ even among similar species, providing complex three dimensional structures and making them difficult to accurately assess using traditional allometric methods. Terrestrial laser scanners (TLS) have been used widely in collecting forest inventory information in recent years, mainly due to their fine-scale, detailed spatial measurements and rapid sampling. In this work we detected stems and roots in TLS data from three mangrove forests on Pohnpei Island in Micronesia using 3D classification techniques. After removing noise from the point cloud, the training set was acquired by filtering the

facets of the point cloud based on angular orientation. However, many mangrove trees contain above-ground roots, which can incorrectly be classified as stems. We consequently trained a supporting classifier on the roots to detect omitted root returns (i.e., those classified as stems). Consistency was assessed by comparing TLS results to concurrent field measurements made in the same plots. The accuracy and precision for TLS stem classification was 82% and 77%, respectively. The same values for TLS root detection were 76% and 68%. Finally, we simulated the stems using alpha shapes for volume estimation. The average consistency of the TLS volume assessment was 85%. This was obtained by comparing the plot-level mean stem volume (m^3/ha) between field and TLS data. Additionally, field-measured diameter-at-breast-heights (DBH) were compared to the lidar-derived DBH using the reconstructed stems, resulting in 74% average accuracy and an RMSE of 7.52 cm. This approach can be used for automatic structural evaluation, and could contribute to more accurate biomass assessment of complex mangrove forest environments as part of forest inventories or carbon stock assessments.

A. Rouzbeh Kargar (✉) · E. Hughes · J. van Aardt
Department of Imaging Science, Rochester Institute of Technology, Rochester, NY 14623, USA
e-mail: axr7139@rit.edu

R. A. MacKenzie
U.S. Forest Service, Pacific Southwest Research Station,
Institute of Pacific Islands Forestry, Hilo,
HI 96720, USA

M. Apwong
University of Hawaii at Hilo, Hilo, HI 96720, USA

Keywords Terrestrial laser scanning · Forest structure · Stem quantification · Mangrove forests

Introduction

Evaluating and monitoring the trends and attributes of biosphere ecology is of significant importance; these trends and attributes in forest environments typically are often assessed via changes in aboveground biomass, annual litterfall, and canopy structure (Saenger and Snedaker 1993). Quantifying above-ground biomass typically involves using allometric equations that are based off of relationships between non-destructive diameter-at-breast-height (DBH) measurements and the sum biomass of tree trunks, branches, and sometimes leaves from a select few trees that have been harvested (Clough and Scott 1989; Fromard et al. 1998). The use of allometric equations is especially challenging in structurally complex forest environments, such as mangrove forests. Allometric equations for mangrove trees often do not include the biomass of complex aboveground root structures that stabilize trees in soft, unconsolidated sediments and in areas of high tidal energy (Duke 1992). Furthermore, complexity and structure can significantly vary among species and between individual trees of the same species (Komiyama et al. 2008). For example, knee roots (Fig. 1a) and pneumatophores (Fig. 1b) project upwards from above sediments; complex networks of prop roots (Fig. 1c), ribbon roots (Fig. 1d), and buttresses (Fig. 1a, d) extend radially. The same allometric equation can therefore introduce significant errors to the assessment of biomass data (Cole et al. 1999). Additionally, the manual data collection for performing such analysis is labor intensive, time consuming, and prone to (subjective) measurement errors. The latter of which can later deteriorate the accuracy and precision of the results. An accurate, efficient, and non-destructive approach is needed to accurately assess and measure the structural characteristics of complex mangrove forest environments.

Improvements in 3D data collection methods for forests have led to more accurate detection and assessment of tree attributes (e.g., location, height, DBH (Bucksch et al. 2013)) and derivation of geometric traits using methods such as cylinder fitting to estimate tree volume (Hopkinson et al. 2004). Since field measurements are time consuming and inefficient, especially in mangrove forests where complex above-ground root structures make data collection more challenging, an increasing number of studies have focused on evaluation of forests using light

detection and ranging (lidar) scans (Yao et al. 2011). As an example, Lefsky et al. (2002) used a single regression model to assess the above-ground biomass in a high biomass forest; such forests traditionally have been regarded as challenging environments for assessment of structural attributes and also carbon storage. The single regression model could explain 84% of the variance in the above-ground biomass, which is a promising result in context of the data and methodology used. Lidar systems rapidly emit laser pulses (> 25 kHz pulse frequency for most terrestrial systems), and measure the return trip elapsed time for each laser pulse to reflect (backscatter) from a target in its path. This elapsed time is converted into a range, distance-from-sensor value, which eventually yields a 3D point cloud of the surrounding environment, typically based on pseudo-hemispherical scan pattern, for terrestrial lidar systems (Baltsavias 1999). Such lidar-based approaches enable us to rapidly and accurately assess plot-level characteristics, e.g., basal area, stem volume, and stem density (Yao et al. 2011) and while would be useful to measure the biomass of complex mangrove forest environments, has rarely used to do so.

One approach for modeling stem structure is by assessing the diameter value at various heights of the tree, i.e., stem taper. While this is a traditional method that uses a relroscope to assess wood volume for timber extraction (Cole et al. 1999), it can also be done by dividing the lidar point cloud into different segments, and then fitting a circle to the area of the stem that is projected onto the horizontal plane (Olofsson and Holmgren 2014). Another method is via fitting a cylinder to 3D segments of the point cloud in order to simulate stems (Thies et al. 2004). In the case of non-circularly shaped stems, free-form curves have been used for modeling the stems (Thies et al. 2004) and also by finding the plane orthogonal to the growth direction of the tree and then projecting the points on this plane, thereby modeling stems that are not perfectly vertical (Forsman and Halme 2005). Another approach relies on a 2D composite of the flattened image of Terrestrial Laser Scanning (TLS) point clouds (Olagoke et al. 2016). Stem modeling has also been performed by using the images of projected point clouds, and detecting the edges and linearity of the stems (Hilker et al. 2013). Voxel-based approaches also have been used for stem volume measurement.

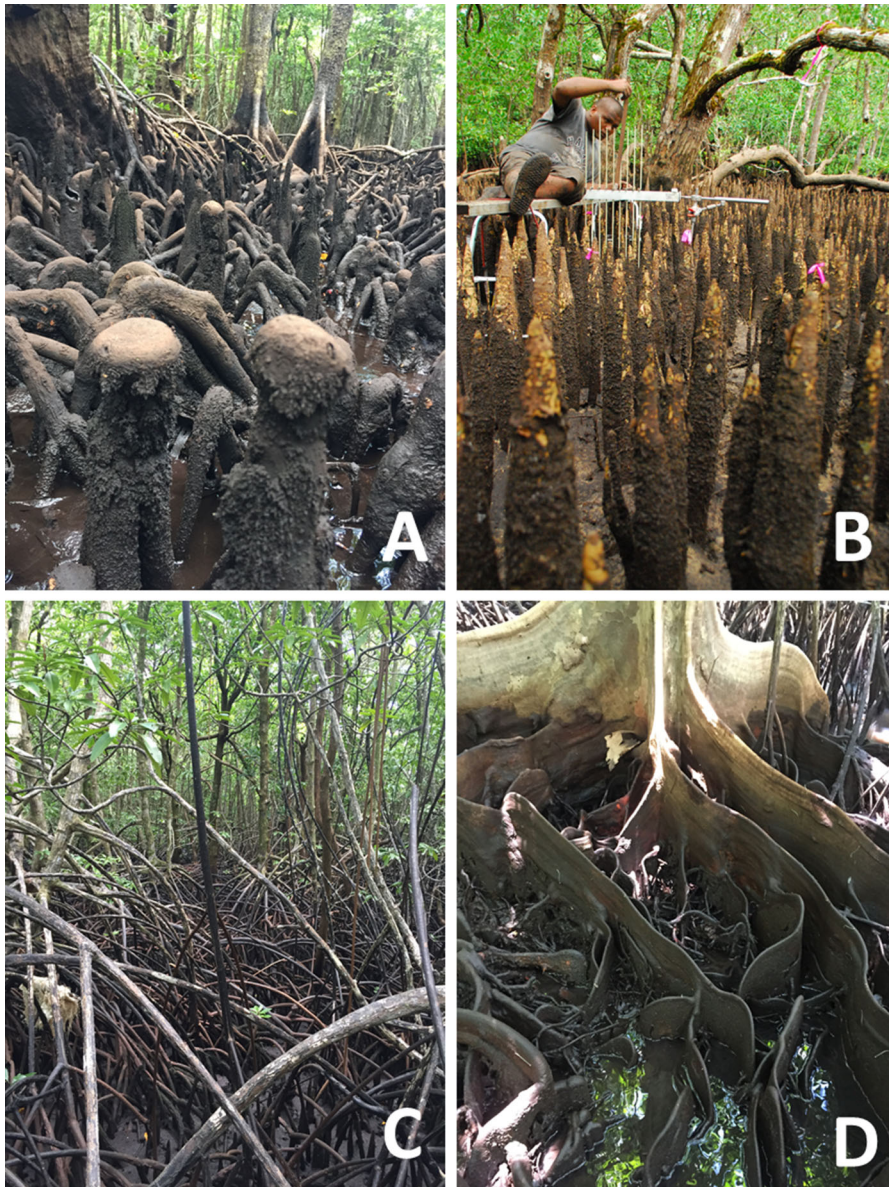


Fig. 1 Structural complexity of mangrove trees that make the development and accuracy of allometric equations challenging. **a** Knee roots and buttress trunks of *Bruguiera gymnorrhiza* (Rhizophoraceae), **b** pneumatophores of *Sonneratia alba*

(Lythraceae), **c** prop/stilt roots of *Rhizophora apiculata* (Rhizophoraceae), and **d** ribbon roots and buttress trunks of *Xylocarpus granatum* (Meliaceae)

Stovall et al. (2017) used a voxelization approach and estimated the trunk volume using the outer hull model (OHM). The OHM uses convex hulls and accurately fits the true shape of the trunk, rather than forcing a cylindrical fit. However, in the case of mangrove stems, which are more structurally complex compared to the data used by the authors (i.e., from pine trees), such an approach could be inaccurate.

These complex forest environments introduce challenges to structural assessment algorithms, thus increasing the need for more advanced techniques.

One example of such a technique is RANdom SAMple Consensus (RANSAC) (Olofsson and Holmgren 2014), which is used for stem detection based on taper models (Page et al. 2009). Advanced algorithms enable us to model the stems more accurately (Kelbe

et al. 2015), while proving useful for associated stem volume assessment (Liang et al. 2012). The lidar-derived forest structural attributes can then be used as inputs to forest biomass, growth, complexity, and structure-composition modeling (Calders et al. 2018).

Prior studies have proven the ability of TLS for tree properties and architecture evaluation. These studies have focused on tree morphology (Janssen et al. 2004), clustering (Delagrange and Rochon 2011), and graph search (Wuttke et al. 2012). Others included voxel analysis methods (Vonderach et al. 2012), which include digitization of the voxel attributes. All these approaches can contribute to our improved management of forests as natural resources (Côté et al. 2011). However, to the best of our knowledge, there is still a lack of studies that have focused on plot-level TLS stem and root assessment in mangrove forests. Most studies on mangrove root and stem assessment are performed on single tree models, acquired from high-density TLS scans (Feliciano et al. 2014; Olagoke et al. 2016), which reduce the confusion for stem and root detection and modeling algorithms.

In this work, we use a low-cost, portable TLS system, the Compact Biomass Lidar (CBL) (Kelbe et al. 2015), which provides rapid 3D scans of its environment. We evaluate this TLS system for detecting stems and assessing their attributes in three different mangrove forests on Pohnpei Island in the Federated States of Micronesia, which we regard as a complex forest environment given the non-circular stem forms, above-ground root mass, and high degree of structural variability in that root mass (Fig. 1). Data collection furthermore is challenging in these mangrove forests due to the locale (access), thus making lightweight, portable scanners more ideal. Such scanners do have a drawback in that they generally provide lower density lidar point clouds than commercial higher-cost scanners, which also introduces challenges to structural assessments based on 3D lidar point clouds. We therefore present an application of classification techniques for automatic detection of tree stems and roots in mangrove forests, based on the structural features of the points, and assess their attributes using geometric reconstruction methods.

Data

Site

Forest plots were previously established in the Enipein, Enipoas, and Sapwalap mangrove forests on the western Pacific island of Pohnpei in the Federated States of Micronesia ($6^{\circ} 50' 59.99''$ N, $158^{\circ} 12' 60.00''$ E). Each plot contained either a surface elevation table or rod surface elevation table (referred to as SET from here on) (see Krauss et al. 2010 for additional details on SETs) that had been installed in 1998 or 2017, respectively. Of the 27 plots, only 18 could be scanned with the lidar. The downward orientation of the scanner arguably could create challenges for forest structural assessment (e.g., occlusion effects for detecting stems) typical for TLS systems in forest environments (Kelbe et al. 2016). However, these drawbacks are mitigated by collecting eight scans per plot, which allowed us to scan specific trees from different locations, thereby enabling offset vantage points and resulting in a dense point cloud.

Compact biomass lidar

The data used in this work were collected using a modified SICK LMS-151 CBL system, a low-cost portable TLS. Such low-cost sensors are designed to address the limitations of TLS in structural evaluation of forests, such as limited mobility, extensive power requirements and prolonged scan times (Van der Zande et al. 2006). The CBL provides us with efficient and rapid sampling of its surroundings (Figs. 2, 3), but with a lower angular resolution and associated point density, compared to higher-cost commercial scanners. As a result, algorithms developed for structural assessment using data from this system need to be robust to issues caused by low-resolution point cloud data. The SICK LMS-151 scanner in the CBL uses a 905-nm laser, pulsing at 27 kHz. The scanning mirror operates in a 270° plane, while the system is attached to a rotation stage, which rotates through 180° , thereby providing coverage for a $270^{\circ} \times 360^{\circ}$ “hemisphere”; as such, only the 90° cone underneath the scanner remains unscanned (Fig. 2). A maximum of two returns are digitized for each lidar pulse that result in two point clouds. The specifications of CBL are presented in Table 1 (SICK AG Waldkirch: Reute 2009). Finally, the CBL was mounted to an inverted

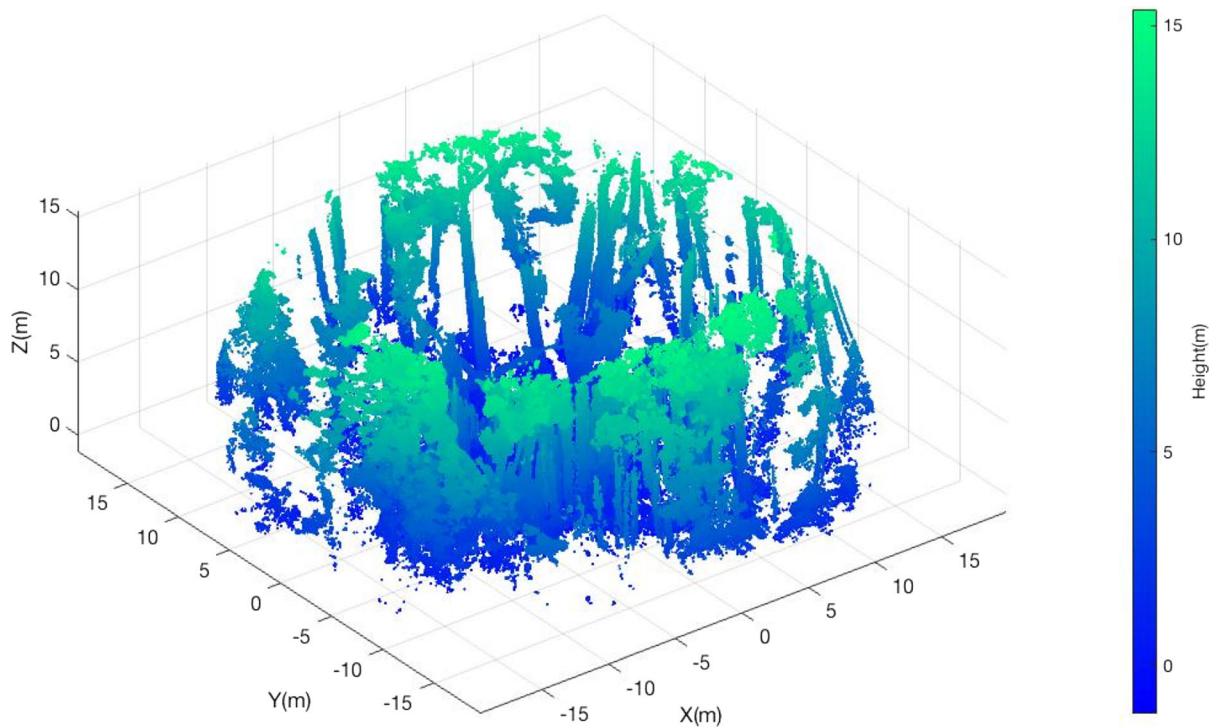


Fig. 2 The height map of a point cloud collected using a terrestrial lidar system. The structures are represented as 3D objects, which can be processed using their coordinates as recorded by the scanner

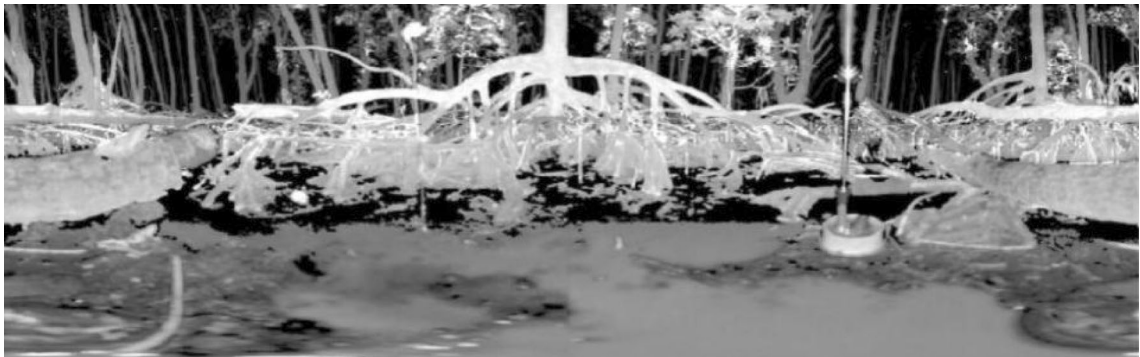


Fig. 3 An intensity image recorded by CBL. The brighter areas represent higher intensity returns, i.e., higher response in 905 nm, and vice versa

extension arm, at a distance of 0.49 m from the plot center, which resulted in each scan location being viewed in a downward fashion; this configuration left a 90° unscanned cone facing directly upward. The scanner mount and configuration were used in this fashion, since the main objective of the field deployment was to assess sediment elevation changes via digital elevation models (DEMs) in the mangrove forests. The focus of this paper, however, was to use

these data to address a secondary objective, namely characterization of the mangrove forest structure.

Field measurement

The CBL system was mounted to each SET receiver in a northward direction prior to scanning the plot (Fig. 1). After each scan, the CBL system was pivoted on the SET receiver 45° clockwise, for a total of eight

Table 1 Specifications of compact biomass lidar instrumentation

Range finder	Time-of-flight and intensity
Wavelength (nm)	905
Maximum range (m)	40
Resolution (°)	0.25
Range accuracy (mm)	30
Scan duration (s)	33
Weight (kg)	3.9
Beam divergence (mrad)	15.0
Minimum angular step-width (mrad)	4.36
Coverage (°)	270*360
Maximum pulse frequency (kHz)	27

scans per plot. The height of the CBL relative to the ground elevation in each plot was dependent on the height of the rSET/SET installation. However, to remove the bias resulting from the measurement height changes, the elevation of the point clouds were normalized using the lidar ground returns for each of the individual plots individually; this facilitated a consistent and accurate approach, one that was independent of the scanner height-above-ground. We installed either 7 m or 10 m radius plots directly adjacent to plots that were scanned with the CBL in order to measure stem volumes in the field. All trees > 5 cm in DBH were identified to species, and DBH was measured to the nearest 0.1 cm within the entire 7 or 10-m radius circular plot. All trees < 5 cm DBH (e.g., saplings) were identified to species and DBH measured to the nearest 0.1 cm within a 2-m radius circular plot, nested within the larger 7 m or 10 m radius subplot. The number of trees measured in each plot ranged between 15 and 21. For trees with prop roots (*Rhizophora* spp.), the point of measurement for determining DBH was 15 cm above the highest prop root that could safely be measured. Species-specific allometric equations developed for Pohnpei (Cole et al. 1999) were then used to estimate tree volume using DBH measurements, after which the volume of each tree was summed for each plot, and the total plot volume within each plot was divided by the area of that plot (m³/ha) (Alexander et al. 2009; Cortes and Vapnik 1995).

Methods

TLS point cloud registration

Scans were co-registered using a combination of manual and automatic methods. First, at each plot, we aligned each pair of consecutively scanned point clouds of the eight total scans based on structural tie points using a pairwise registration technique, which provides us with a rigid transformation matrix as the output (Zai et al. 2017). The Iterative Closest Point (ICP) algorithm was then used as part of the registration process to improve the registration accuracy. For each lidar return in the 3D point cloud, the ICP algorithm matches the closest point in the reference point cloud and evaluates a combination of rotation and translation parameter values between the two, using the root mean square distance minimization technique (Besl and McKay 1992). All eight scans were registered in each plot, forming one combined 3D point cloud (Fig. 2). Since the area right above the scanner has an artificially high point density (i.e., where multiple scan lines intersect, thereby oversampling this location), we downsampled the point cloud to normalize the density distribution and remove any CBL sampling bias from our results. The downsampling technique in our work is based on the spherical sampling of the data and considers lower weight for points closer to the scanner and higher weights for those further away, thereby ensuring that 3D sampling remains unbiased (no scanner protocol impacts) and that the structural variability of the point cloud is maintained (van Aardt et al. 2017; Fafard et al. 2020).

Noise removal

After registering the scans, we needed to remove the noise returns in the point cloud in order to improve the performance of our classification. Typically, lidar data contain sparse outliers, which can decrease the structural evaluation accuracy, and can also complicate estimation of local point characteristics, like normal or curvature changes. For this step, we used the Statistical Outlier Removal (SOR) algorithm (Rusu et al. 2008). SOR is based on the distribution of distances between a point and its neighbors. For each point, the mean distance to all the neighboring points is computed, and based on an assumption of a Gaussian distribution, all of the points with a mean distance outside a set threshold are considered outliers. This threshold is defined by the mean and standard deviation of the global distances between the points in the data. The number of neighbors we used for SOR assessment in this study was five, which was determined by the point density, ranging from 1700 to 3200 points/m³, in the structures of the point cloud we needed to maintain. We evaluated the density in manually detected stems that were further from the scanner, but where we could still represent the geometric structure of the stem accurately, and identified the number of points that best preserved these structures after application of the SOR noise removal algorithm.

Higher canopy removal

The next step was to remove the higher canopy points, since while most TLS systems provide detailed 3D scans of the fine-scale, close-range below-canopy environment, the laser signal attenuates (reflected, absorbed, transmitted, and occluded) toward the upper-canopy layers (Côté et al. 2009). The removal of upper-canopy layers therefore was necessary since the objective of this work focused on assessment of below-canopy structures (i.e., stems), and the higher canopy may contribute to confusion during structural evaluation of the stem and root components. Removal of upper canopy lidar returns was achieved via normal change rate assessment. The normals of the point cloud, which are unit vectors perpendicular to the plane fitted to the points, differ in terms of angular orientation and also change rates in stems and forest canopies. The normal difference of the canopy point

cloud is generally smaller than non-canopy segments, due to more structural irregularity in these areas (Rouzbeh Kargar et al. 2019; Li et al. 2017). The remaining segments contained the stems and roots, following detection and removal of the canopy lidar returns from the point cloud.

Stem and root classification

Stem and root detection in complex forest environments is challenging due to the high structural complexity and variability of these structures. Another challenge we face in this study is the low-density 3D (point cloud) data. Such lower density data, relative to longer-scanning, more expensive scanners, can negatively affect both classification and reconstruction. These impacts can be accentuated in root evaluation, because of the higher variability in shape and structural complexity. Additionally, acquiring accurate information about these structures using only allometric equations is challenging, due to the above-mentioned reasons. As a result, an automated approach to detect, evaluate, and reconstruct stems and roots in Mangrove forests is ideal for extending the application and interpretation of allometric equations, or with further improvements, to be used as a stand-alone method. Details on the detection methods in this work and results are presented in the following sections.

Building the training set

We used a 3D classifier (Shapovalov and Velizhev 2011), in order to detect the stems in the segmented section of the point cloud. First, we needed to construct the training set for this classifier. We extracted the facets of the point cloud (i.e., the planar surfaces between adjacent lidar returns) to find the angular distribution of the points (Dewez et al. 2016) using kd-Tree and Fast Marching in the FACETS plugin in CloudCompare software (v 2.9.1; Bentley 1975; Sethian 1996; Dewez et al. 2016). Kd-Tree is a method for partitioning the data in order to arrange points in k-dimensional space, and Fast Marching is a numerical approach for finding the boundary values. Both of these algorithms subset the point cloud into segments, find the planar surfaces, and then propagate them into polygons (enclosed areas/units). A tension parameter is used in order to modify the boundaries of

these segmented planes; this parameter operates by moving the vertices closer to, or away from, the neighboring vertices, based on the distance between the points and finding the average position of the neighboring vertices. This is done to acquire smoother boundaries and less artifacts in these regions. The difference between the FACETS method and other similar approaches (e.g., curvature filtering) is that the segmentation part of this method using Kd-tree and Fast Marching, helps to reduce the run time in “big data”, such as the 3D point clouds used in this study. Additionally, due to the structural complexity of these data (i.e., the above-ground roots, small gaps between structures), the more advanced segmentation step used in FACETS can improve the results compared to similar methods.

We determined that the stem facets’ angular distribution was between 77° and 112° , after analyzing the facetized point cloud. This was obtained by manually investigating the plots and extracting 20 facets for stems per plot, specifically the stems that represented extreme angular orientations (Fig. 4).

The 3D classifier

We used a 3D lidar point cloud classification technique, introduced by Shapovalov and Velizhev (2011), to classify roots and stems in the processed point clouds. In this approach, a spatial index first is assigned to each point in the training set; in our case, the index was set for stem points that were detected by filtering the facets of the point cloud using their angular orientation. All other points were labeled as “non-stem”. This stage introduces over-segmentation, the segmented sections of the point cloud are themselves partitioned into subsets. The algorithm builds a graph over the segments, after labeling the points, and then the features are extracted. This classifier then trains the Random Forest classifier (Ho 1995) on the point features of specific classes (i.e., roots and stems). Subsequently, a kernelized structural support vector machine (Bertelli et al. 2011) is used for estimating the dependency of the points. As stated before, the training set was obtained by filtering the facets of the point cloud, based on the estimated angular

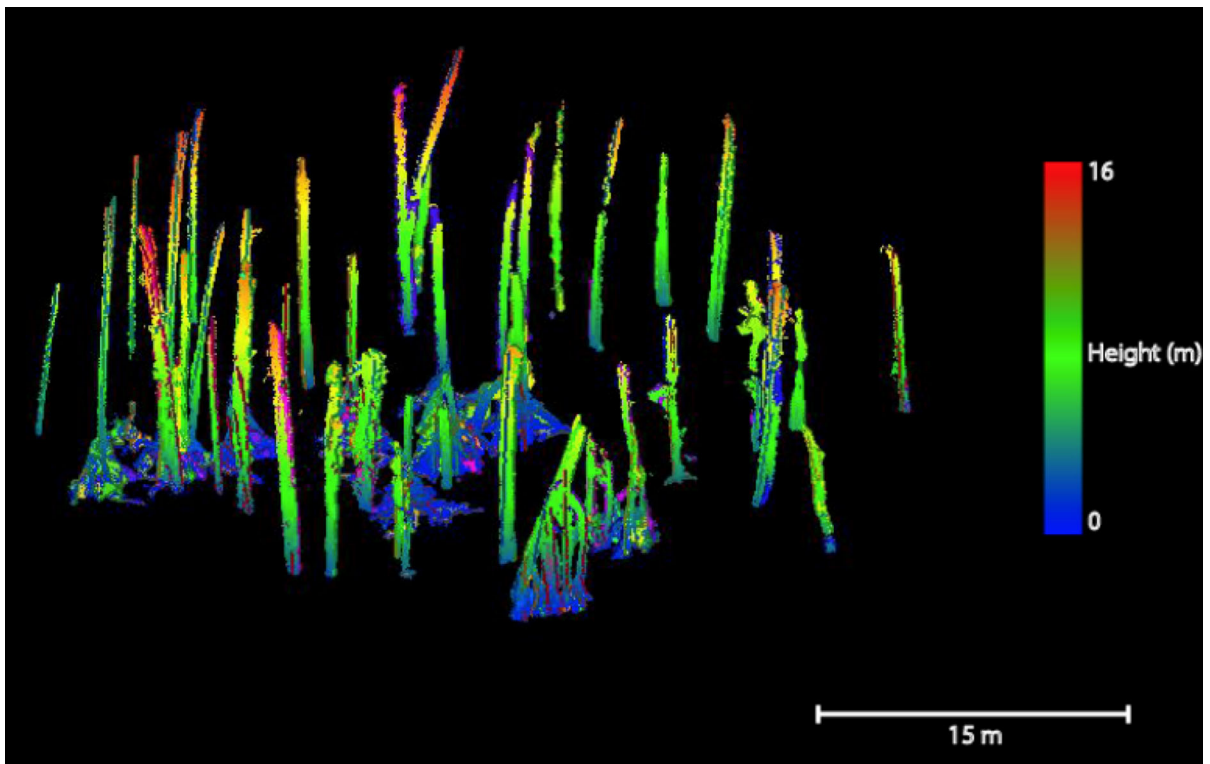


Fig. 4 The height map of the facetized point cloud of the stems and roots. It can be seen that the stems are more vertically oriented, while the roots, shown in the lower portion of the point cloud in blue (colder) colors, are more horizontally oriented

distribution of the stem facets. The stems detected using this approach in 15 plots were used as the training set. It is important to mention that not all the stems in the plot were detected using the filtering of the facets, and as a result, the training set did not include all the stems in these plots. This is due to the fact that in the areas where the stem points were very close to other structures, the facet extracted from the stem was unified with other structures, resulted in a different angular orientation and direction. Consequently, after filtering out the facets, some of these stem points were removed.

The initial result of the classification included some incorrectly labeled points as stems. These points mostly belonged to the typical above-ground roots found in mangrove forest ecosystems. We therefore trained a supporting classifier on the root points. The same approach was followed for training the root point classifier; however, in order to remove any bias in our method, we gathered our training set for the root points from the same plots that we used for the stem classification.

Stem reconstruction and volume measurement

The next step, after detecting stems and roots, was to measure the volume of the stems. We simulated the detected stems using alpha shapes (Akkiraju et al. 1995). Alpha shapes are linear simple curves in the Euclidean plane, related to the shape of a set of points (Edelsbrunner et al. 1983). The difference between an alpha shape and a convex hull is that one can incorporate a shrinkage factor in the alpha shape approach, thus implying that a convex hull is an alpha shape with zero shrinkage (Fig. 5). In other words, three dimensional convex hull polygons are known to overestimate the object volume, so introducing supplementary geometric metrics, or a shrinkage factor in this case, can improve the results (Paynter et al. 2018). We found that shrinkage factor of 0.3 yielded the most accurate result. This was determined based on comparing the polylines, resulting from the projection of the points of the stems and those obtained from projecting the reconstructed stems using alpha shapes, with different shrinkage factors. The points closer to the scanner were used for this component of our approach, since the higher point density in these regions resulted in a more detailed 3D sampling of the

environment. This finding also was validated by comparing the area of the projected stems.

CBL data validation

Tree volume consistency assessment

The stem volume data obtained from lidar were then compared to the field-measured volume data. The reported volume (m^3/ha) for lidar data in each plot was found by summing the volumes of all the detected stems, and then dividing by the area in which the stems were detected, for a circular area with radius of 7 m or 10 m, based on the radius used for field measurement:

$$\text{Volume} = \sum_{i=1}^n \frac{v_i}{\text{area}}$$

where n is the number of detected stems in the plot, v is the volume of each stem (m^3), and area is the area of the plot (ha).

DBH assessment

In our final step, we evaluated the DBH using the lidar point clouds to have a more reliable metric to compare our field measurements with and validate our methodology. DBH was measured 15 cm above the highest prop root for each tree stem in the field. We followed the same approach using the reconstructed stems from lidar point clouds. After detecting the stems and roots, and simulating the stems, we segmented the points from 14 cm to 16 cm height range from the base of the stem model. This range was introduced to address the bias and error in field measurement of DBH and the sparsity of the lidar data. Afterwards, these points were projected on the X Y plane and a circle was fit to them, for which the diameter represents the DBH (Fig. 6).

Results and discussion

Results

Stem and root classification accuracy assessment

We trained a classifier on the stems and a supporting one on the roots (Fig. 7) as discussed above.

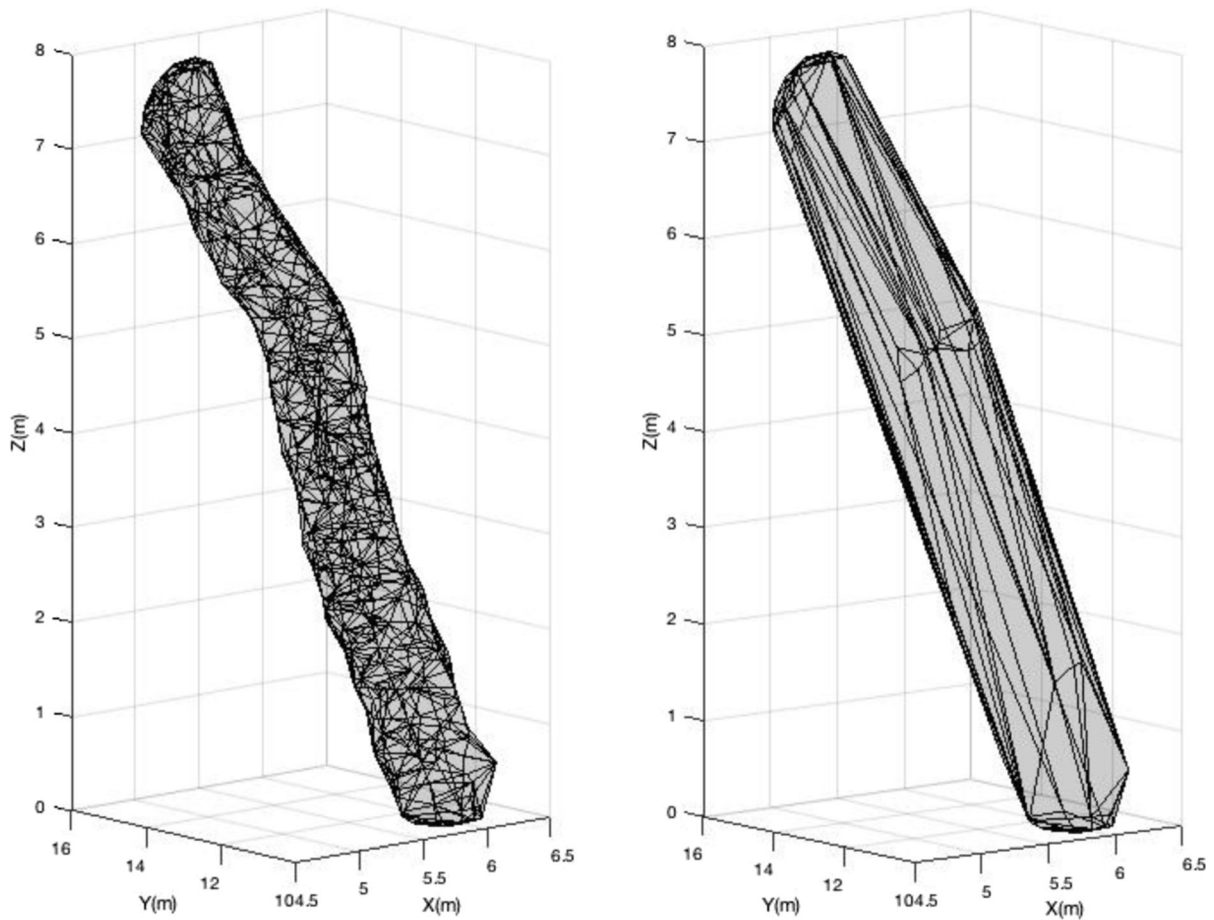


Fig. 5 The image on the left shows a stem reconstruction using an alpha shape with a shrinkage factor of 0.3, while the image on the right shows the same stem, simulated using a convex hull.

The classification results contained some noise points, such as sparse points which did not belong to the structures in the lidar point cloud, and some errors such as roots were labeled as stems, that were attributed to the complex structure of the mangrove forest. The accuracy of this classification therefore was assessed using the true and false positive and negative values (Li and Guo 2013) in each plot. These were found via manual investigation, where the results of classification were manually validated by inspecting the point clouds, and the following formula was used for calculating the accuracy:

$$Accuracy = \frac{tp + tn}{tp + tn + fp + fn}$$

where tp denotes true positive, tn is true negative, fp is false positive, and fn shows false negative values. Classification precision was also calculated using the following equation:

$$Precision = \frac{tp}{tp + fp}$$

Table 2 shows the result of the accuracy assessment of this classification.

The accuracy of the root classification is lower than for the stem classification, which was attributed to the more complex structure of the roots and more structural diversity in their shapes and orientations. When the structural complexity increases (e.g., due to

We found that the shrinkage factor of 0.3 models the stems more accurately for our study environment

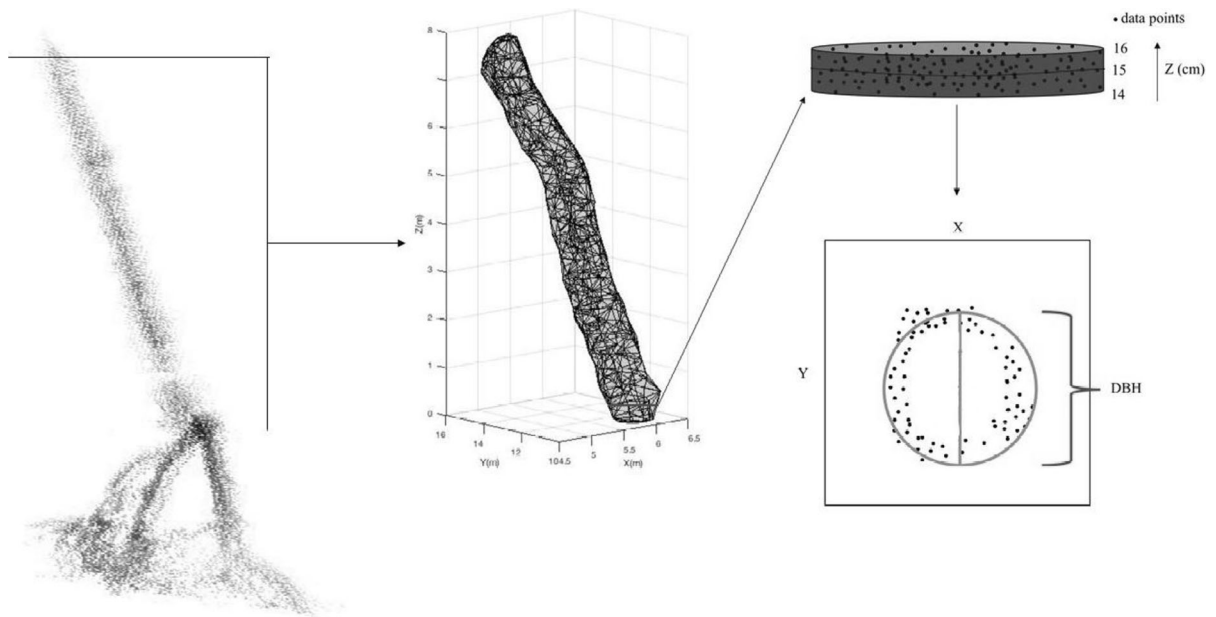


Fig. 6 The measurement of DBH using reconstructed stems from lidar point clouds. The root points (shown in the point cloud on the left) are segmented out after classification, after which the DBH measurement is performed on the stems

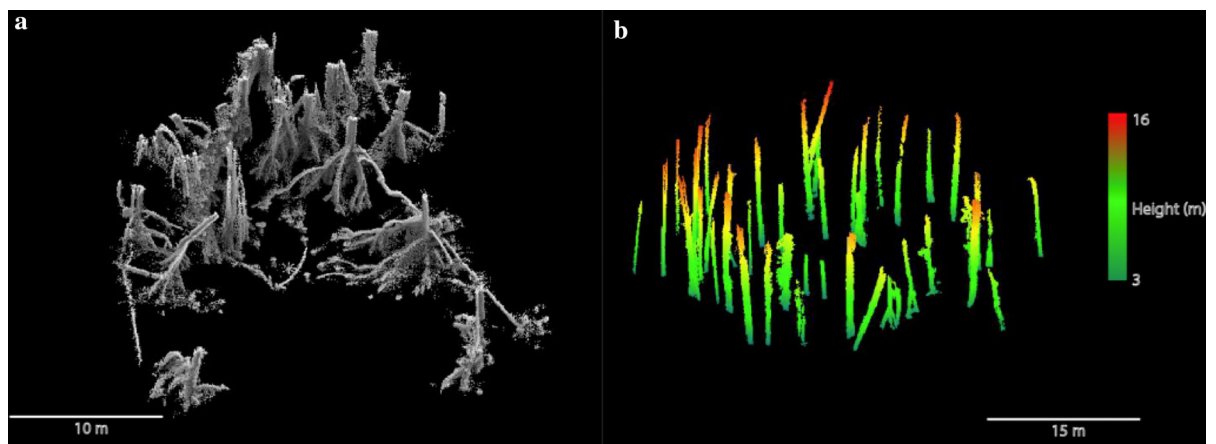


Fig. 7 Result of root and stem classification in one of the plots, **a** a top-down view of the detected roots, and **b** the height map of the detected stems. The maximum height of the stems in this plot was found to be 14 m

Table 2 Accuracy assessment results for stem and root classification

Task	Accuracy (%)	Precision (%)
Stem classification	82	77
Root detection	76	68

more complex root shapes) reduced distances between different segments of the roots, and more rapid angular

orientation changes of these segments, the extraction of distinct features becomes more challenging for the classifier, thereby resulting in a lower classification accuracy.

Stem volume measurement consistency assessment

In our next step, we used alpha shapes to reconstruct the tree stems. We observed that the selected

shrinkage factor of 0.3 avoided overestimation of stem volumes (Fig. 8).

As mentioned before, we calculated stem volumes for each plot for all the trees within a 7 m or 10 m radius from the center scanner location, based on the radius used in the field-measured data. This was done to avoid the lower point densities beyond this radius, and to compare volume/ha to the field measurements that were also made. The lower far-range point densities of TLS are due to angular divergence of scan lines, attenuation of laser energy, both as a function of range-from-scanner, and occlusion effects (Dix et al. 2011). We constructed stem volumes up to a maximum height of 12 m, since the average point density for the stems was significantly lower after this height, less than 15% of the total stem density. The plot-level field-measured stem volume ranged between 91.71 and 1105.5 m³/ha, while the lidar-

derived plot-level stem volume ranged from 105.36 to 1014.4 m³/ha. The average consistency of stem volume measured using the CBL was within 85% of the volumes estimated from DBH measurements made in the field, ranging from 66 to 98% across plots. The RMSE value was 63.65 m³/ha, with a MAE value of 49.89 m³/ha. The consistency in this case was found using the following equation:

$$\text{Consistency} = \frac{\text{Field value} - |\text{Field value} - \text{lidar value}|}{\text{Field value}}$$

where *Field Value* denotes the field measured stem volume, and *Lidar Value* is the volume data acquired from lidar point clouds. It is important to note that although more effective, it was not possible to compare volume measurement between the manual

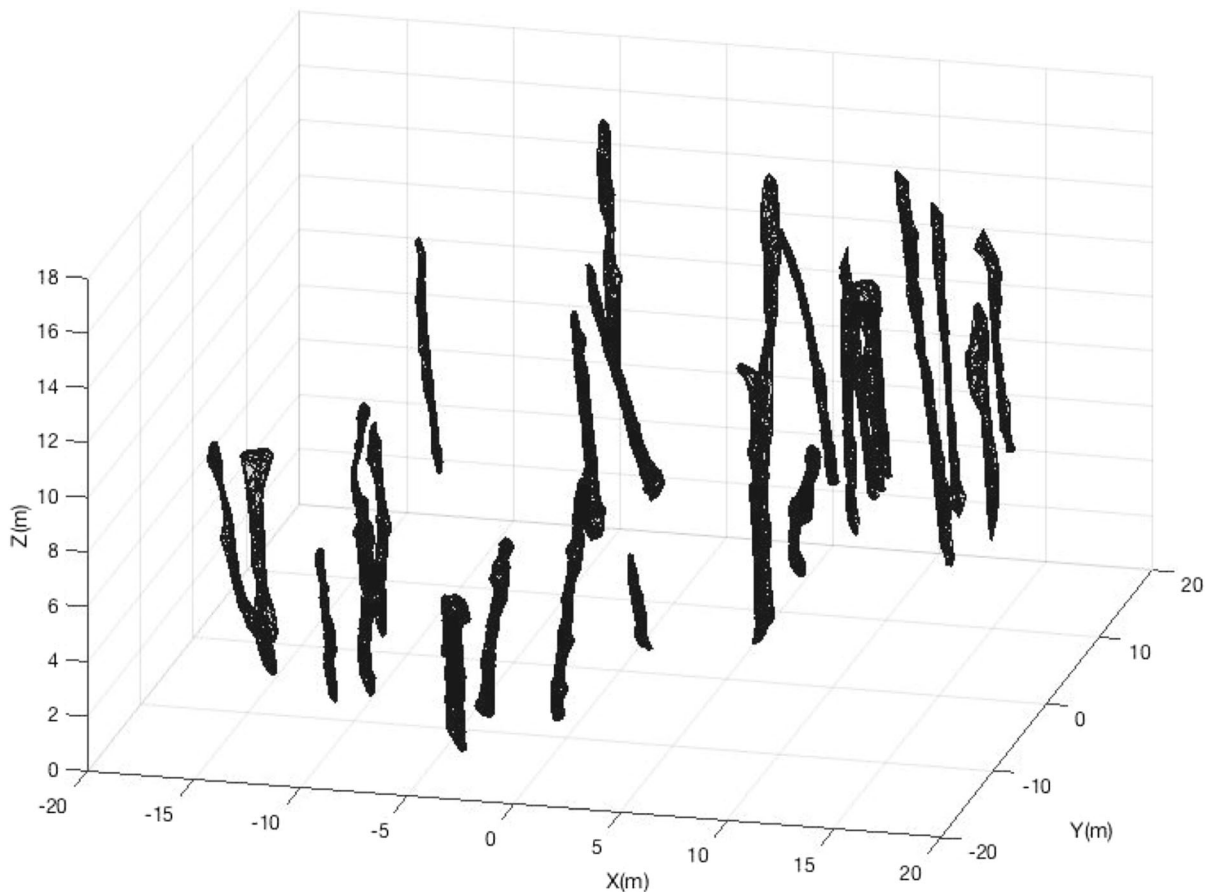


Fig. 8 The result of reconstructing tree stems using alpha shapes in one plot. The stems that were within a radius of 7 m or 10 m from the scanner, based on the radius of the field measurement, were included in the analysis for volume measurement

and lidar approach at the tree level, since the stem map information was not available. As a result, the plot-level volume measurement comparison was applied.

DBH and basal area evaluation accuracy assessment

The DBH accuracy was assessed using the same formula used in “[Stem volume measurement consistency assessment](#)” section. Table 3 represents the DBH evaluation results.

The accuracy was assessed in each plot and the average accuracy is the result of averaging all the acquired per plot accuracy values. It is important to note that since the stem map was not available for this data, the DBH values were compared on a plot level.

We applied Kolmogorov–Smirnov (KS) test (Stephens 1974) to test whether the difference between the field-measured DBH and lidar-derived DBH is statistically significant. The KS test is a nonparametric approach for comparing the similarity of two probability distributions. We chose this approach because we did not have any underlying assumptions regarding the probability distribution of the data. The result showed a p value of 0.131 at the critical value of 0.05. We therefore concluded that the difference between the two sets of data is not statistically significant.

We also generated a basal area estimate, using DBH extracted from lidar-derived DBH values. We found an average consistency of 88% and RMSE of 6.06 m²/ha, when comparing the field-measured basal area and the lidar-derived result. Table 4 shows both the plot-level and species-level field-measured stem density, basal area, and tree volume and the plot-level lidar-derived basal area and tree volume. The species are listed as: (i) RHSP, which represents *Rhizophora apiculata*, *Rhizophora mucronate*, and *Rhizophora stylosa*, (ii) SOAL (*Sonneratia alba*), (iii) XYGR (*Xylocarpus granatum*), and (iv) BRGY (*Bruguiera gymnorhiza*).

Discussion

One challenge in this work is the relatively low-density data, which require algorithms to be robust to this aspect, both for pre-processing and classification. The low-density data decrease the classification, and subsequent volume estimation and DBH evaluation accuracies. We should place this in context though—the data used here are not sub-standard, but rather the result of a portable, low power requirement (e.g., industry-standard power tool batter pack), lower-cost, and rapid-scan system, which makes it significantly more practical for further utilization in complex forest environments. The variation in DBH assessment accuracy and tree volume consistency between plots was attributed to the spatial complexity across site locations, i.e. the diversity in root shapes, stems’ angular orientation, and vegetation density. Accuracy was lower in the plots where the vegetation density was higher, and the structure of the above-ground roots were more complex in terms of angular, shape, and size diversity, thus making the feature extraction of stems more challenging. For example, two plots are shown in Fig. 9 from the same site, one with less structural complexity in above-ground root shapes (Fig. 9a) and the other with higher structural complexity in above-ground roots and dense vegetation (Fig. 9b). The consistency of stem detection was lower in the specific plot with higher complexity, by 12%. This was attributed to an increased occlusion effect, and a reduced distance between the stems and higher-elevated root structures. In the latter case, when extracting the facets of the point cloud for gathering training set, the stem segments and those of roots are associated with one single plane, which can introduce errors to the classification, leading to less accurate detection and volume estimation per plot. The angular orientation of the stems was another issue that caused a decrease in classification and stem volume accuracies. After further assessment we found that most of the stems that were incorrectly classified had an angular

Table 3 Accuracy assessment results for DBH evaluation

Field-measured DBH range (cm)	Lidar-derived DBH range (cm)	Average accuracy	RMSE (cm)
16.8–41.8	19.2–52.6	74%	7.52

Table 4 Sum of stem densities, tree basal area, and tree volume for each species and plot, sampled using standard US Forest Service methods and the terrestrial lidar

Site	Stem density	Tree basal area (m ² /ha)	Tree volume (m ³ /ha)
<i>Enipein</i>			
Fringe A	0.8	11.53	75.4
RHSP	0.3	5.90	49.2
BRGY	0.5	5.63	26.1
Lidar		10.60	98.93
Fringe B	1.5	16.59	82.7
RHSP	0.5	5.64	30.4
BRGY	1	10.95	52.3
Lidar		14.86	101.74
Fringe C	1.9	16.46	83.1
RHSP	0.9	7.329	34.8
SOAL	0.1	1.98	13.6
BRGY	0.9	7.15	34.7
Lidar		14.79	91.22
Riverine A	2.2	79.06	571.3
RHSP	0.8	12.07	93.5
SOAL	0.1	45.56	365.0
BRGY	1.3	21.42	112.8
Lidar		80.42	579.72
Riverine B	0.6	7.68	44.7
RHSP	0.1	1.36	10.1
XYGR	0.3	1.00	4.5
BRGY	0.2	5.30	30.1
Lidar		6.24	50.36
Riverine C	1.4	47.77	323.9
BRGY	0.5	11.36	62.8
RHSP	0.5	5.30	38.4
XYGR	0.4	31.11	222.8
Lidar		33.01	358.81
<i>Enipoas</i>			
Fringe A	1.8	25.62	139.3
RHSP	0.3	1.070	5.4
SOAL	0.1	3.90	27.6
BRGY	1.4	20.65	106.3
Lidar		27.49	164.91
Fringe B	2.2	74.87	522.0
RHSP	0.3	2.40	15.8
SOAL	0.8	53.98	408.6
BRGY	1.1	18.48	97.6
Lidar		79.13	577.82
Fringe C	3	67.93	482.9
RHSP	2.1	21.33	148.8
SOAL	0.4	38.48	290.9
BRGY	0.5	8.1	43.1
Lidar		66.51	541.72
Interior A	2.7	49.80	308.5

Table 4 continued

Site	Stem density	Tree basal area (m ² /ha)	Tree volume (m ³ /ha)
RHSP	0.7	7.09	48.5
SOAL	0.2	19.89	151.2
BRGY	1.8	22.82	108.7
Lidar		46.8	381.31
Interior B	2.6	59.56	392.5
RHSP	0.9	6.66	41.6
SOAL	0.4	35.51	264.7
BRGY	1.3	17.38	86.2
Lidar		68.4	421.69
Interior C	2.1	48.53	328.2
RHST	0.3	6.78	66.2
SOAL	0.3	16.34	117.8
BRGY	1.5	25.40	144.1
Lidar		46.97	372.37
Riverine B	1.8	45.73	323.7
RHSP	1.1	16.42	127.9
SOAL	0.1	17.01	129.7
BRGY	0.6	12.29	66.1
Lidar		50.81	362.91
Riverine C	1.3	44.55	278.4
BRGY	1.3	44.55	278.4
Lidar		41.46	304.31
<i>Sapwalap</i>			
Fringe B	2.8	25.68	156.7
RHSP	2	14.80	98.4
XYGR	0.7	9.75	53.2
BRGY	0.1	1.13	5.1
Lidar		38.91	188.12
Fringe C	1	51.98	387.6
RHSP	0.1	3.80	38.7
SOAL	0.2	37.21	285.3
XYGR	0.7	10.96	63.6
Lidar		55.83	311.48
Interior A	0.7	25.29	216.1
RHSP	0.4	13.34	139.7
BRGY	0.3	11.95	76.4
Lidar		22.01	226.53
Interior B	1.6	63.54	493.3
RHSP	1.2	18.99	159.2
SOAL	0.2	39.12	300.7
XYGR	0.1	0.96	4.8
BRGY	0.1	4.47	28.5
Lidar		54.18	386.6

orientation near the extreme limits, i.e. 77° and 112° —in these cases some of the stems were incorrectly classified as roots. To address this issue, additional scans can be collected in the areas where the stems are occluded (“shadowed”) by above-ground roots and more dense vegetation. These scans can be collected in different angular directions, or even different spatial positions. We studied the relationship between the ratio contribution of the most complex species, i.e. *Rhizophora*, with the plot-level basal area and tree volume accuracy. Although we could not find a significant relationship, we argue that if a stem map were available and the data could be compared at the tree-level, we likely would observe the largest disparity between the measured volume and basal area in the plots with the highest *Rhizophora* ratio contribution, due to the higher structural complexity of this species. This is another question that can be assessed in future work.

Additionally, in the case of DBH evaluation, an average overestimation of 25% was observed in the lidar DBH values. This was due to the errors in reconstructed stems, caused by our relatively low-density 3D data. Additionally, this was attributed to the errors caused by simulating the segments of the stems that were occluded from the scanner’s view.

Although the use of eight 45° displaced scans per plot, all with different viewsheds, arguably minimizes lidar shadowing and occlusion effects, these are still present and can introduce errors in reconstructing stems for volume and DBH measurement. However, this occlusion is a typical drawback of all terrestrial laser scanners, and can only be circumvented by displacing the scanner significantly between adjacent scans. We were constrained by the fixed plot location in this study, where the CBL was physically attached to an SET receiver. We were able to offset the scanner 0.49 m from the plot center via an extension arm, and then rotate the instrument through a full 360° at 45° increments. This set-up arguably negates some detrimental occlusion effects, but given the non-cylindrical nature of mangrove stems, the complex above-ground root mass, and the non-vertical nature of much of the forest structure, we recommend that future studies also investigate an approach where the scanner is displaced by > 5 m between adjacent scans.

Conclusions

We presented an approach for stem detection and volume measurement in complex mangrove forest



Fig. 9 Images of two of the plots where the data were collected, **a** contains less structural complexity, resulting in a higher accuracy for stem detection and volume estimation, and **b** the

high-elevated complex structure of above-ground roots reduced the accuracy of stem classification and volume estimation in this plot

environments, by applying machine learning and geometric reconstruction techniques to terrestrial lidar system data (light detection and ranging; 3D point clouds). Such complex forest environments introduce challenges to automatic structural evaluation algorithms, mainly due to large variance in angular, size class, and shape distributions of both stems and roots, with the latter often presenting above ground, further creating class confusion. We presented methods for overcoming these challenges, by (i) reducing the confusion for the algorithm via removal of upper-canopy lidar returns and facet-based distribution analysis and (ii) automating the assessment of the structural attributes, via angular assessment of point cloud facets and the use of alpha shapes to model stems. We obtained accuracies of 76% and 82% for root and stem classification, respectively, while our stem volume assessment matched allometric-based measurements at an 85% level, on average.

Mangrove forests contain distinct structural features, such as complex above-ground roots and non-circular stems forms, making their evaluation different than other types of forest environments. The results show that this methodology is effective at providing a relatively accurate estimation of the volume data ($\sim 85\%$ consistency), which can then be used as an input for biomass modeling, detailed structural assessment of the forest, and even for change detection. We could also argue that the TLS-based method in fact provides a more accurate volume estimation, when compared to manual approaches. This is due to the fact that using TLS, we can provide an accurate 3D model of the stems and measure their volume that incorporate irregularities in the stem not captured using traditional allometric equations that assume stems are essentially perfect cylinders or tapers and that typically only use a single diameter as a parameter for volume estimation. However, the result is affected by the structural complexity, which includes the diversity in above-ground roots structural attributes, non-vertical stem forms, and vegetation density of the plot, where a decrease in accuracy was observed in plots that exhibited more complexity in terms of lidar point density. We contend that this challenge can be overcome by collecting higher number of scans in areas where the stems are shadowed by above-ground roots, or including a pre-processing step in which the vegetation is segmented from the woody materials in the scene. The latter can be done in a more accurate

way using a dual wavelength scanner, to be able to differentiate between the foliar and non-foliar returns more effectively. Even though future work could focus on refinement of this approach to address these shortcomings, the results still bode well for rapid, accurate, and precise characterization of these valuable and rapidly changing ecosystems. Such a TLS scanning approach effectively can be used to rapidly characterize remote locations, thereby reducing field sampling time and impacts, while serving as calibration data for more synoptic air- and spaceborne structural sensing of mangrove forests.

Acknowledgements This research was funded in part by United States Forest Service, Pacific Southwest Research Station, and United States Geological Survey (USGS; award # G19AC00355). The opinions expressed are those of the authors, and not those of either the USFS or USGS.

Funding This research was funded in part by United States Forest Service, Pacific Southwest Research Station, and United States Geological Survey (USGS; Award # G19AC00355). The opinions expressed are those of the authors, and not those of either the USFS or USGS.

Compliance with ethical standards

Conflict of interest The authors declare that they have no conflict of interest.

References

- Akkiraju N, Edelsbrunner H, Facello M, Fu P, Mucke EP, Varela C (1995) Alpha shapes: definition and software. In: Proceedings of the 1st international computational geometry software workshop, vol 63, p 66
- Alexander C, Smith-Voysey S, Jarvis C, Tansey K (2009) Integrating building footprints and LiDAR elevation data to classify roof structures and visualise buildings. *Comput Environ Urban Syst* 33(4):285–292
- Baltsavias EP (1999) Airborne laser scanning: basic relations and formulas. *ISPRS J photogramm Remote Sens* 54(2–3):199–214
- Bentley JL (1975) Multidimensional binary search trees used for associative searching. *Commun ACM* 18(9):509–517
- Bertelli L, Yu T, Vu D, Gokturk B (2011) Kernelized structural SVM learning for supervised object segmentation. In: CVPR 2011. IEEE, pp 2153–2160
- Besl PJ, McKay ND (1992) Method for registration of 3-D shapes. In: Sensor fusion IV: control paradigms and data structures. International Society for Optics and Photonics, vol 1611, pp 586–607
- Bucksch A, Lindenbergh R, Rahman MZA, Menenti M (2013) Breast height diameter estimation from high-density

- airborne LiDAR data. *IEEE Geosci Remote Sens Lett* 11(6):1056–1060
- Calders K, Origo N, Disney M, Nightingale J, Woodgate W, Armston J, Lewis P (2018) Variability and bias in active and passive ground-based measurements of effective plant, wood and leaf area index. *Agric For Meteorol* 252:231–240
- Clough BF, Scott K (1989) Allometric relationships for estimating above-ground biomass in six mangrove species. *For Ecol Manag* 27(2):117–127
- Cole TG, Ewel KC, Devoe NN (1999) Structure of mangrove trees and forests in Micronesia. *For Ecol Manag* 117(1–3):95–109
- Cortes C, Vapnik V (1995) Support-vector networks. *Mach Learn* 20(3):273–297
- Côté JF, Widlowski JL, Fournier RA, Verstraete MM (2009) The structural and radiative consistency of three-dimensional tree reconstructions from terrestrial lidar. *Remote Sens Environ* 113(5):1067–1081
- Côté JF, Fournier RA, Egli R (2011) An architectural model of trees to estimate forest structural attributes using terrestrial LiDAR. *Environ Model Softw* 26(6):761–777
- Delagrange S, Rochon P (2011) Reconstruction and analysis of a deciduous sapling using digital photographs or terrestrial-LiDAR technology. *Ann Bot* 108(6):991–1000
- Dewez TJ, Girardeau-Montaut D, Allanic C, Rohmer J (2016) Facets: a cloudcompare plugin to extract geological planes from unstructured 3D point clouds. *Int Arch Photogramm Remote Sens Spat Inf Sci*, vol 41
- Dix M, Abd-Elrahman A, Dewitt B, Nash L Jr (2011) Accuracy evaluation of terrestrial LiDAR and multibeam sonar systems mounted on a survey vessel. *J Surv Eng* 138(4):203–213
- Duke NC (1992) Mangrove floristics and biogeography. In: Robertson AI, Alongi DM (eds) *Tropical mangrove ecosystems*. American Geophysical Union, Washington, DC, pp 63–100
- Edelsbrunner H, Kirkpatrick D, Seidel R (1983) On the shape of a set of points in the plane. *IEEE Trans Inf Theory* 29(4):551–559
- Fafard A, Rouzbeh Kargar A, van Aardt J (2020) Weighted spherical sampling of point clouds for forested scenes. *Photogramm Eng Remote Sens* (in-press)
- Feliciano EA, Wdowski S, Potts MD (2014) Assessing mangrove above-ground biomass and structure using terrestrial laser scanning: a case study in the Everglades National Park. *Wetlands* 34(5):955–968
- Forsman P, Halme A (2005) 3-D mapping of natural environments with trees by means of mobile perception. *IEEE Trans Rob* 21(3):482–490
- Fromard F, Puig H, Mougouin E, Marty G, Betoulle JL, Cadamuro L (1998) Structure, above-ground biomass and dynamics of mangrove ecosystems: new data from French Guiana. *Oecologia* 115(1–2):39–53
- Hilker T, Frazer GW, Coops NC, Wulder MA, Newnham GJ, Stewart JD et al (2013) Prediction of wood fiber attributes from LiDAR-derived forest canopy indicators. *For Sci* 59(2):231–242
- Ho TK (1995) Random decision forests. In: *Proceedings of 3rd international conference on document analysis and recognition*. IEEE, vol 1, pp 278–282
- Hopkinson C, Chasmer L, Young-Pow C, Treitz P (2004) Assessing forest metrics with a ground-based scanning lidar. *Can J For Res* 34(3):573–583
- Janssen LLF, Gorte BGH (2004) Digital image classification. In: *Principles of remote sensing: an introductory textbook*. ITC, Chicago, pp 193–204
- Kelbe D, van Aardt J, Romanczyk P, van Leeuwen M, Cawse-Nicholson K (2015) Single-scan stem reconstruction using low-resolution terrestrial laser scanner data. *IEEE J Sel Top Appl Earth Obs. Remote Sens.* 8(7):3414–3427
- Kelbe D, van Aardt J, Romanczyk P, van Leeuwen M, Cawse-Nicholson K (2016) Marker-free registration of forest terrestrial laser scanner data pairs with embedded confidence metrics. *IEEE Trans Geosci Remote Sens* 54(7):4314–4330
- Komiyama A, Ong JE, Pongpan S (2008) Allometry, biomass, and productivity of mangrove forests: a review. *Aquat Bot* 89:128–137
- Krauss KW, Cahoon DR, Allen JA, Ewel KC, Lynch JC, Cormier N (2010) Surface elevation change and susceptibility of different mangrove zones to sea-level rise on Pacific high islands of Micronesia. *Ecosystems* 13(1):129–143
- Lefsky MA, Cohen WB, Harding DJ, Parker GG, Acker SA, Gower ST (2002) Lidar remote sensing of above-ground biomass in three biomes. *Glob Ecol Biogeogr* 11(5):393–399
- Li W, Guo Q (2013) A new accuracy assessment method for one-class remote sensing classification. *IEEE Trans Geosci Remote Sens* 52(8):4621–4632
- Li S, Dai L, Wang H, Wang Y, He Z, Lin S (2017) Estimating leaf area density of individual trees using the point cloud segmentation of terrestrial LiDAR data and a voxel-based model. *Remote Sens* 9(11):1202
- Liang X, Hyypä J, Kaartinen H, Holopainen M, Melkas T (2012) Detecting changes in forest structure over time with bi-temporal terrestrial laser scanning data. *ISPRS Int J Geo-Inf* 1(3):242–255
- SICK, LMS100/111/120/151 Laser Measurement Systems Operating. Instructions (2009) SICK AG Waldkirch: Reute, Germany
- Olagoke A, Proisy C, Féret JB, Blanchard E, Fromard F, Mehlig U et al (2016) Extended biomass allometric equations for large mangrove trees from terrestrial LiDAR data. *Trees* 30(3):935–947
- Olofsson K, Holmgren J (2014) Forest stand delineation from lidar point-clouds using local maxima of the crown height model and region merging of the corresponding Voronoi cells. *Remote Sens Lett* 5(3):268–276
- Page S, Hoscilo A, Wösten H, Jauhainen J, Silvius M, Rieley J, ... Limin S (2009) Restoration ecology of lowland tropical peatlands in Southeast Asia: current knowledge and future research directions. *Ecosystems* 12(6):888–905
- Paynter I, Genest D, Peri F, Schaaf C (2018) Bounding uncertainty in volumetric geometric models for terrestrial lidar observations of ecosystems. *Interface Focus* 8(2):20170043
- Rouzbeh Kargar A, MacKenzie R, Asner GP, Van Aardt J (2019) A density-based approach for leaf area index assessment in a complex forest environment using a terrestrial laser scanner. *Remote Sens* 11(15):1791

- Rusu RB, Marton ZC, Blodow N, Dolha M, Beetz M (2008) Towards 3D point cloud based object maps for household environments. *Robot Auton Syst* 56(11):927–941
- Saenger P, Snedaker SC (1993) Pantropical trends in mangrove above-ground biomass and annual litterfall. *Oecologia* 96(3):293–299
- Sethian JA (1996) A fast marching level set method for monotonically advancing fronts. *Proc Natl Acad Sci* 93(4):1591–1595
- Shapovalov R, Velizhev A (2011) Cutting-plane training of non-associative markov network for 3D point cloud segmentation, 3D imaging, modeling, processing, visualization and transmission (3DIMPVT), vol 8
- Stephens MA (1974) EDF statistics for goodness of fit and some comparisons. *J Am Stat Assoc* 69(347):730–737
- Stovall AE, Vorster AG, Anderson RS, Evangelista PH, Shugart HH (2017) Non-destructive aboveground biomass estimation of coniferous trees using terrestrial LiDAR. *Remote Sens Environ* 200:31–42
- Thies M, Pfeifer N, Winterhalder D, Gorte BG (2004) Three-dimensional reconstruction of stems for assessment of taper, sweep and lean based on laser scanning of standing trees. *Scand J For Res* 19(6):571–581
- van Aardt J, Fafard A, Kelbe D, Giardina C, Selmants P, Litton C, Asner GP (2017) A terrestrial lidar's assessment of climate change impacts on forest structure. *Silvilaser 2017*. October 10–12, 2017; Blacksburg, VA
- Van der Zande D, Hoet W, Jonckheere I, van Aardt J, Coppin P (2006) Influence of measurement set-up of ground-based LiDAR for derivation of tree structure. *Agric For Meteorol* 141(2–4):147–160
- Vonderach C, Voegtle T, Adler P (2012) Voxel-based approach for estimating urban tree volume from terrestrial laser scanning data. *Int Arch Photogramm Remote Sens Spat Inf Sci* 39:451–456
- Wuttke S, Schilling H, Middelman W (2012). Reduction of training costs using active classification in fused hyperspectral and lidar data. In: *Image and signal processing for remote sensing XVIII*. International Society for Optics and Photonics, vol 8537, p 85370 M
- Yao T, Yang X, Zhao F, Wang Z, Zhang Q, Jupp D (2011) Measuring forest structure and biomass in New England forest stands using Echidna ground-based lidar. *Remote Sens Environ* 115(11):2965–2974
- Zai D, Li J, Guo Y, Cheng M, Huang P, Cao X, Wang C (2017) Pairwise registration of TLS point clouds using covariance descriptors and a non-cooperative game. *ISPRS J Photogramm Remote Sens* 134:15–29

Publisher's Note Springer Nature remains neutral with regard to jurisdictional claims in published maps and institutional affiliations.